AQUA
Water Infrastructure, Ecosystems and Society



IWA PUBLISHING

 AQUA — Water Infrastructure, Ecosystems and Society Vol 73 No 3, 584 doi: 10.2166/aqua.2024.311

# Analysis of land use/land cover changes and driving forces during the period 1992–2022: a case study of Jinan City, China

Lingye Tan, Robert Tiong L. K. and Ziyang Zhang*
School of Civil and Environmental Engineering, Nanyang Technological University, Singapore 639798, Singapore
*Corresponding author. E-mail: ziyang004@e.ntu.edu.sg

## ABSTRACT

This research aims to quantify the spatial pattern of urban land use/land cover (LULC) change while considering environmental effects. This paper integrates historical Landsat imagery, The Environment for Visualizing Images (ENVI), geographical information system (GIS), and socio-economic data to determine the spatial–temporal urban LULC dynamics and the conversion of LULC in response to the rapid urbanization from 1992 to 2022. Principle component analysis and multiple linear regression are used to determine and model the relationship between the socioeconomic factors and the changes for identifying the driving forces. The results indicate that impervious surfaces have exponentially increased, expanding more than two times from 2,348 to 4,795 km$^2$, in contrast to bare lands, which drastically declined by 95%, from 1,888 to 87 km$^2$. Water bodies have always been relatively fewer, at approximately 100 km$^2$. In addition, the majority of farmland in Jinan City is concentrated in the northern region with a steady area in the range of 2,100–2,900 km$^2$, while the majority of woodland located in the southern region declined from 3,774.52 km$^2$ (37%) to 3,088.28 km$^2$ (30%). Economic development, population growth, and climate change are the primary factors that have an obvious impact on LULC changes.

**Key words:** driving factors, land use/land cover dynamic change, remote sensing, spatial pattern, transition

## HIGHLIGHTS

- This paper integrates remote sensing images, ENVI, geographical information system, and socioeconomic data to determine the spatial–temporal urban land use/land cover.
- Principle component analysis and multiple linear regression are used to determine the relationship between the socioeconomic factors and the changes for identifying the driving forces.
- The results indicate a rocketing increase of impervious surfaces, which expanded more than two times from 2,348 to 4,795 km$^2$.

## 1. INTRODUCTION

The alteration of land use/land cover (LULC) is the most direct indication of the impact of human activities on the Earth's surface system and plays a crucial role in the process of global environmental change (Wulder *et al.* 2008; Mooney *et al.* 2013; Lawler *et al.* 2014). Through interactions with the biosphere and atmosphere, human activities directly or indirectly influence surface albedo, surface energy, surface roughness, and evapotranspiration, leading to significant effects on the surface radiation energy balance, biogeochemical cycles, and ecosystem services (Deng *et al.* 2014; Zhu & Woodcock 2014). Additionally, LULC is a critical factor in determining human responses to global change and serves as a vital input parameter for simulating global climate and biogeochemical effects. Understanding its spatio-temporal process and dynamic mechanism, and accurately measuring and simulating its changes, have become top priorities in scientific research (Jin *et al.* 2019; Debnath *et al.* 2022; Gaur & Singh 2023). The alteration of LULC patterns can result from a plethora of driving forces, including urbanization, economic growth, and natural calamities. As a result, it is imperative to study the changes in LULC at both the temporal and spatial scales to gain a comprehensive understanding of the underlying mechanisms driving these changes. The temporal analysis focuses on the examination of LULC changes over time, including the evolution of the extent and distribution of various LULC types. Contrarily, the spatial analysis examines how various LULC types are arranged and patterned, as well as how they relate to one another. In China, research on LULC has primarily focused on examining the changing patterns, driving mechanisms, and environmental impacts of land use at

the regional level (Wear & Bolstad 1998; Yu & Yang 2002; Hietel *et al.* 2004). The selected areas typically fall into two main categories. The first category comprises 'fragile areas' that are characterized by vulnerable ecological environments, which are often found in unique geographic locations such as coastal areas (Zhu *et al.* 2022), plateaus (Wang *et al.* 2022), or delta regions (Zhang *et al.* 2020). The second category includes 'hot spot areas' with high levels of human activities and natural drivers, which are often found in international metropolises such as Beijing, Shanghai, or Guangzhou (Yin *et al.* 2011; Ding & Shi 2013; Wu *et al.* 2016). The diverse purposes and patterns of land use lead to changes in LULC that are influenced by various factors. Understanding the forces driving land-use change is crucial to addressing land system-related challenges. Scholars have different views regarding these factors, generally classifying them into natural geographic and socioeconomic factors (Sanderson *et al.* 2002; Hersperger & Bürgi 2009; Arifasihati 2016). Some researchers emphasize demographic factors such as population growth (Nagy & Lockaby 2011; Tiitu 2018; Tavares *et al.* 2019), population density (Xu *et al.* 2013; De la Luz Hernández-Flores *et al.* 2017), and rural-to-urban migration as key drivers of LULC change (Essien & Cyrus 2019; Islam *et al.* 2021). On a macro-scale, factors such as climate change and soil processes play significant roles but tend to have long-term and stable effects, accumulating over time. At the regional level, socioeconomic factors have a more pronounced impact (Stephen *et al.* 1993; Turner *et al.* 1993; Briassoulis & van der Straaten 2000; Xie *et al.* 2005).

Remote sensing (RS) has become a reliable monitoring tool for LULC changes because of the increasingly diverse and high-quality RS databases that meet various research needs. The availability of MODIS, Landsat, and Sentinel images has made RS imagery interpretation research more efficient and cost-effective. Academic studies show that image processing and classification methods have improved accuracy (Lu *et al.* 2011; Shao & Lunetta 2012; Thanh Noi & Kappas 2017; Toure *et al.* 2018). Numerous studies at local, national, continental, and global scales show that RS and spatial analysis in geographical information systems (GISs) enable fast and efficient LULC change detection. Some studies examined local areas (Wu *et al.* 2006; Rawat & Kumar 2015; Tadese *et al.* 2020), while others examined national issues (Sánchez-Cuervo *et al.* 2012; Schoeman *et al.* 2013). Overall, the amalgamation of RS and spatial analysis techniques in GISs, coupled with advancements in image processing and classification techniques, has simplified and made the monitoring of land-use changes more cost-effective.

Jinan, the capital of Shandong Province and one of China's 14 mega cities, holds a strategic geographical position, situated between the capital economic circle in the north, the Yangtze River Delta economic circle in the south, the Shandong Peninsula in the east, and Central China in the west. Benefiting from substantial national resources and favorable policies, Jinan has experienced rapid development in recent years, becoming a prominent example of swift urbanization and industrialization over the last three decades. In 2022, Jinan's gross domestic product (GDP) grew by 3.1% year-on-year and the economic growth rate is 0.1% higher than the national average rate, which ranks eighth among all cities.

While research on land-use change is prevalent, the current studies investigating the characteristics of land-use change in China have predominantly centered on first-tier cities such as Beijing, Shanghai, and Guangzhou (Yin *et al.* 2011; Ding & Shi 2013; Wu *et al.* 2016), as well as on a national scale (Jiyuan *et al.* 2002; Li *et al.* 2018). Previous research on the Jinan region mainly focused on various ecosystems and specific resources, such as examining the changes in groundwater supply in the Jinan spring area, exploring the atmospheric particulate pollution and water pollution due to LULC (Sun *et al.* 2016). However, few studies have focused on long-term (30 years) LULC changes and analyses of driving factors in the Jinan region. In addition, few scholars have taken policy factors into account in land research in the Jinan region. The policies and regulations issued by the government are among the factors that cannot be ignored due to their impact on sudden land-use changes (Feng & Wang 2021). Numerous scholars have highlighted the significance of institutional elements, particularly local government policies (Xu *et al.* 2013; Kontgis *et al.* 2014; Nassar *et al.* 2014), rules and regulations (Dai *et al.* 2018; Tiitu 2018; Feng & Wang 2022), and alternations in the ownership of land (Zhang *et al.* 2015; Adam 2019; Whiteside 2020), which can influence the trends of the development of cities. Thus, it is meaningful and valuable to fill the research gaps and analyze the LULC changes over the past three decades, including the several factors and policies behind these changes.

The study delivers detailed information on Jinan's LULC change characteristics between 1992 and 2022. The land resource management department can create planning strategies based on the quantitative and spatial variations of LULC. These strategies aim to detect the regional properties of LULC variations and optimize the utilization of farmland, forest, bare land, and impervious surfaces accordingly. In addition, farmland and woodland should be protected to encourage sustainable development in Jinan, lessen farmland fragmentation, and enhance the woodlands in terms of quality (refers to condition and

characteristics of the woodland such as the health and diversity of tree species, the density of trees, and the age structure of the forest) and quantity (refers to the extent or size of the woodland). Additionally, finding the main LULC driving factors can spur land management organizations to develop focused land control plans. It is anticipated that the study's findings will deepen our understanding of how the changes take place and what impact they have, offering insightful information for efficient land resource management and planning. Hence, the primary goals of this paper are (i) to analyze and depict the primary LULC changes in the Jinan region over a 30-year period beginning in 1992; (ii) to investigate the impact of major driving factors, such as GDP or population, on these LULC changes; and (iii) to assess the key implications of these changes by principle component analysis (PCA), analyzing them in the context of national and local policies.

## 2. STUDY AREA AND DATASETS

### 2.1. Study area

Jinan (36° 40′ N, 116° 57′ E) is the provincial capital of Shandong (Figure 1). It is situated in the province of Shandong's northwestern region. The city is located in a region that divides the Yellow River valley from the northern foothills of the Taishan Massif. Numerous artesian springs can be found throughout the metropolitan area thanks to the karst aquifers in limestone formations that slope north to south. A humid continental climate and a normal isotherm of 3°C result in a yearly average temperature of 14.70°C (58.5°F) for Jinan. This city has direct control over six districts (Shizhong, Lixia, Tianqiao, Huaiyin, Licheng, and Changqing), one county-level city (Zhangqiu), and three counties (Pingyin, Jiyang, and Shanghe). All the districts are depicted in Figure 1.

### 2.2. Dataset acquisition

The USGS Earth Explorer, accessible through the official website earthexplorer.gov, provides the essential satellite data (Landsat-8 OLI and Landsat-5TM) required for analyzing changes in LULC in Jinan. The Landsat-5 TM data and the Landsat-8 OLI data offer a 30 m resolution. To ensure greater accuracy in determining the period, the period from April to September is generally selected as the weather is generally good and the cloud content is low. Additionally, all satellite imagery data include cloud cover below 5%, which can plummet differences between months and improve the precision of the classification process by the random forest (RF) method. In this research, seven images were downloaded from USGS, which are related to Landsat 5-TM (Type 1) and Landsat-8 OLI (Type 2). Information related to Band 1–Band 7 (B1–B7) of Type 1 is used, whereas for Type 2, B1–B11 is applied (Table 1).

Data regarding these driving factors were derived from the Jinan Municipal Bureau of Statistics (http://jntj.jinan.gov.cn/). Regional LULC change is caused by a variety of factors, according to research. LULC change is primarily impacted by the development of cities and the economical states (Dewan & Yamaguchi 2009). High correlations between the amount of developed land and arable land in a region and its economic growth have been found (Tendaupenyu *et al.* 2017). China has a dual urban–rural structure, and as a result, the infrastructure, employment opportunities, educational attainment, and access to healthcare in urban and rural areas differ significantly. These variations encourage rural residents to relocate to urban areas, which is a primary factor in the change in regional LULC. Therefore, we selected the three main factors that determine the population: permanent population (PP), urban population (UP), and population density (POD). As a result of the economy's growth and increasing salaries, the government invested in facilities and raised the living standards in urban districts, which raised the area available for impervious surfaces and decreased the amount of farmland. Likewise, the expansion of residential construction and infrastructure would substantially boost the Fixed Assets Investment (FAI). As a result, we settled on GDP and FAI as the key factors at the level of economic development. In addition, climate change can also affect LULC, such as the selection and scope of farmland and forest land. We selected annual temperature (AT) and annual rainfall (AR) as the driving forces at the level of climate change. The annual GDP value-added signifies the level of economical enhancement (unit: 109 yuan). Furthermore, other factors such as UP, population pressure (PP), POD, urban income (UI), and farmers income (FI) are listed in Table 2.

## 3. METHODS

Figure 2 shows the methodology followed by this paper. After aquiring suitable Landsat images, we used ENVI 5.3 for image pre-processing before using the Landsat images for classification. We then carried out the classification and spatial analysis to describe the spatio-temporal pattern of LULC in Jinan City in 1992–2022. The relationship between the change of LULC and

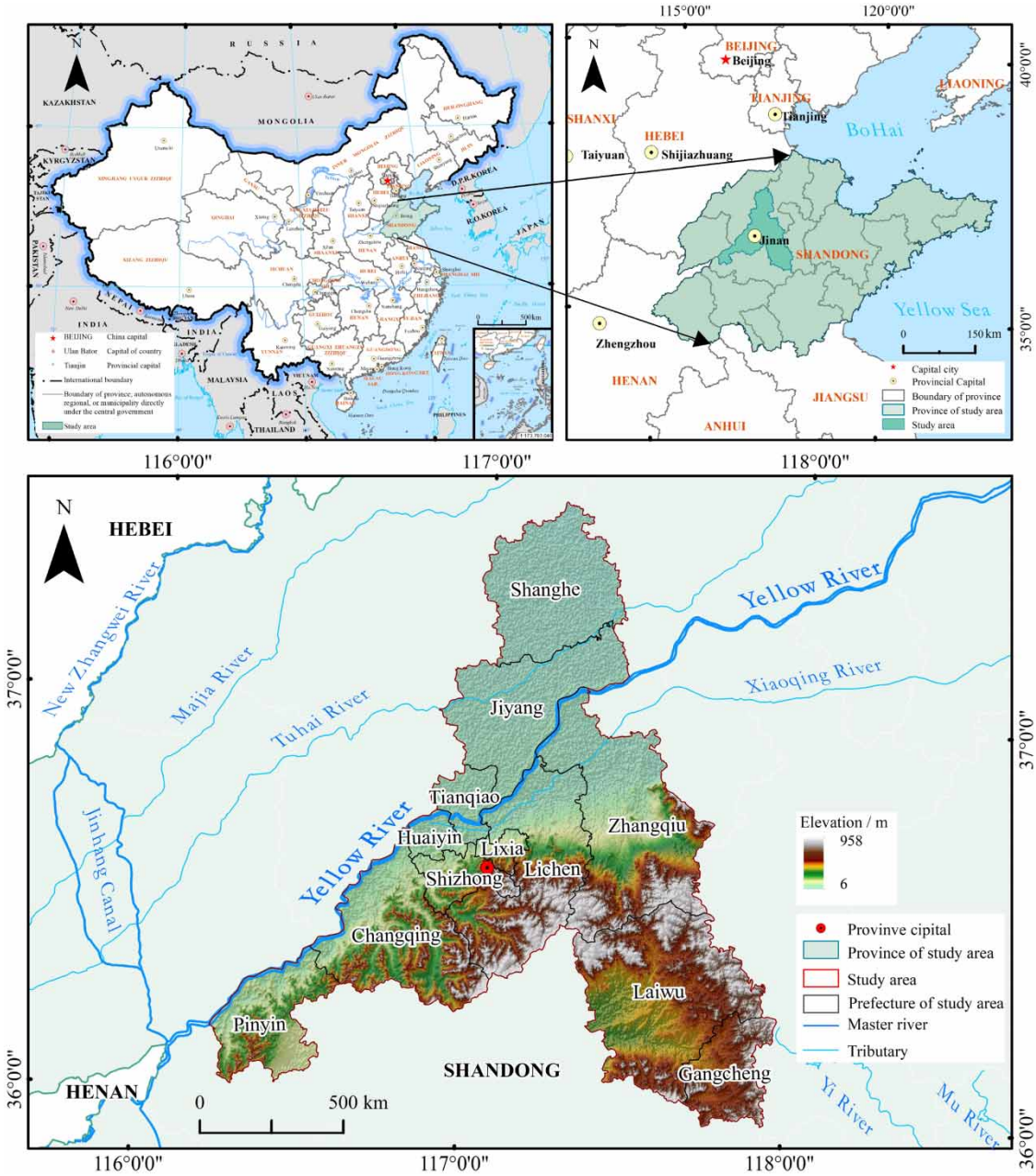


**Figure 1** | Research area map.

multiple factors was explored. We used PCA to reduce the dimensionality of the impacting factors and regression to study how changes in the potential influential factors affected the evolution of LULC in Jinan City.

### 3.1. Image interpretation

The Jinan City region consists of farmland (wheat, rice, sugarcane, etc.), forest, urban and rural impervious surfaces, and water bodies (rivers, canals, and ponds). Five LULC classes have been determined for this study after a review of the literature. Using the ENVI 5.3 Tool, the set of training area classes is created by selecting polygons for each class. The spectral properties and responses are used to separate these LULC classes. The region of interest tool is utilized for assessing spectral variations within defined pairs of LULC classes and demonstrated significant levels of separability between regions of interest. Table 3 displays RS image interpretation symbols.

**Table 1** | Comprehensive details of the Landsat satellite imagery applied in this research

| Acquirement date | Source of data | Dataset | Resolution (m) | Cloud cover | Band | Geographical coordinate system | Projection coordinate system |
|---|---|---|---|---|---|---|---|
| 27/05/1992 | USGS | Landsat 5-TM | 30 | <5% | B1–B7 | GCS_WGS_1984 | UTM_Zone_50N |
| | USGS | Landsat 5-TM | 30 | <5% | B1–B7 | GCS_WGS_1984 | UTM_Zone_50N |
| 28/05/1998 | USGS | Landsat 5-TM | 30 | <5% | B1–B7 | GCS_WGS_1984 | UTM_Zone_50N |
| | USGS | Landsat 5-TM | 30 | <5% | B1–B7 | GCS_WGS_1984 | UTM_Zone_50N |
| 23/05/2002 | USGS | Landsat 5-TM | 30 | <5% | B1–B7 | GCS_WGS_1984 | UTM_Zone_50N |
| | USGS | Landsat 5-TM | 30 | <5% | B1–B7 | GCS_WGS_1984 | UTM_Zone_50N |
| 02/05/2006 | USGS | Landsat 5-TM | 30 | <5% | B1–B7 | GCS_WGS_1984 | UTM_Zone_50N |
| | USGS | Landsat 5-TM | 30 | <5% | B1–B7 | GCS_WGS_1984 | UTM_Zone_50N |
| 16/05/2011 | USGS | Landsat 5-TM | 30 | <5% | B1–B7 | GCS_WGS_1984 | UTM_Zone_50N |
| | USGS | Landsat 5-TM | 30 | <5% | B1–B7 | GCS_WGS_1984 | UTM_Zone_50N |
| 16/05/2017 | USGS | Landsat 8 OLI | 30 | <5% | B1–B11 | GCS_WGS_1984 | UTM_Zone_50N |
| | USGS | Landsat 8 OLI | 30 | <5% | B1–B11 | GCS_WGS_1984 | UTM_Zone_50N |
| 30/05/2022 | USGS | Landsat 8 OLI | 30 | <5% | B1–B11 | GCS_WGS_1984 | UTM_Zone_50N |
| | USGS | Landsat 8 OLI | 30 | <5% | B1–B11 | GCS_WGS_1984 | UTM_Zone_50N |

**Table 2** | Statistical summary of the independent factors related to LULC variation

| Factors | Description |
|---|---|
| GDP | The value-added of GDP each year, which represents economic development level (unit: $10^9$ yuan) |
| PP | The total registered population of the city each year, which represents population pressure (unit: $10^4$) |
| UP | People residing in urban area for each year, which represents urbanization level (unit: $10^4$) |
| POD | Resident population per unit area, which represents population pressure (unit: /$km^2$) |
| FI | Represents capability of improve living conditions of urban residents (unit: yuan) |
| UI | Represents capability of improving living conditions of farmers (unit: yuan) |
| FAI | Represents capability of fixed assets investment (unit: $10^9$ yuan) |
| AT | Represents the average AT (unit: °C) |
| AR | Represents the average annual rainfall (unit: mm) |

### 3.2. Preprocessing stage of images

Due to the errors of the sensor itself and the refraction or absorption of the solar radiation entering the atmosphere, all of the factors produce different degrees of impact on the received signal of the sensor, so a series of preprocessing steps should be performed before applying the RS images of the study area, to improve the accuracy of the interpretation. In this study, we used ENVI 5.3 for image processing, which contains several steps: radiation calibration, atmospheric correction, image mosaic, and image cropping. In Figure 2, the entire LULC workflow is depicted.

Radiometric calibration, also referred to as radiometric correction, is essential for successfully converting unprocessed digital image data from satellite or aerial sensors to a typical physical scale based on known reflectance measurements acquired from objects' surfaces on the ground (Pourazar *et al.* 2019). This type of correction is essential for obtaining accurate quantitative assessments of imagery. The objective of atmospheric correction is to eliminate atmospheric effects from RS satellite images, allowing for the retrieval of surface reflectance. This crucial process is essential for quantitative RS, as it reduces atmospheric interference. Problems with atmospheric disturbance are resolved by using the Fast Line-of-Sight Atmospheric Analysis of Spectral Hypercubes (FLAASH) atmospheric correction technique, which eliminates absorption brought on by

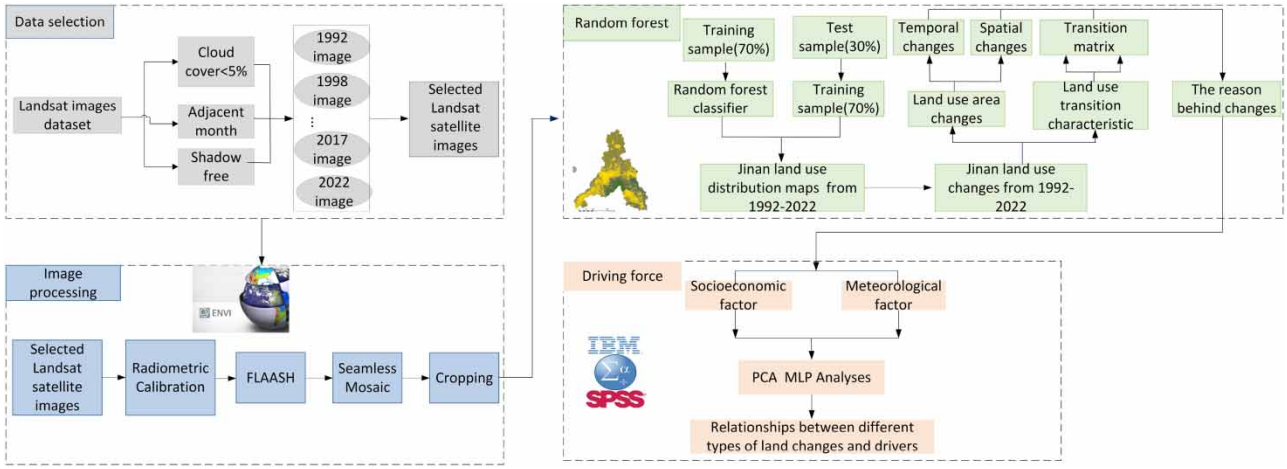


**Figure 2** | Workflow of LULC change based on RF classification.

**Table 3** | RS image interpretation symbols

| No. | Classification types | Implications | Image example | Image features |
|---|---|---|---|---|
| 1 | Farmland | Land on which crops are grown, including watered land, dry land, grassland, shrubs |  | True color images are green and divided into blocks of regular shapes by roads, generally surrounded by residential areas |
| 2 | Impervious surfaces | Includes urban sites and villages |  | Standard false color images show red with white dots and gray with blue, both in aggregates |
| 3 | Water bodies | Including rivers, lakes, and ponds |  | Dark blue on standard false color images, curved, or irregularly shaped |
| 4 | Woodland | Woodland and other forestlands | 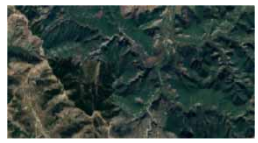 | Red and irregularly shaped on standard false color images, distributed in mountainous areas |
| 5 | Bare land | Low-coverage areas, unused land |  | Irregular brownish-yellow color on true color images, mostly located in mountainous areas |

the effects of $CO_2$, $O_2$, $O_3$, and water vapor as well as the scattering brought on by molecules and aerosols (Chen *et al.* 2011). When extracting information from imagery data obtained under different conditions based primarily on spectral features, such as when detecting changes or mapping vegetation using extensive multi-temporal Landsat imagery data, atmospheric

correction is particularly crucial. Image mosaic and image cropping are the processes of stitching multiple adjacent images that contain parts of the study area into one image that completely covers the study area, and then cropping the desired area according to the study boundary data.

Additionally, a single RS map cannot completely cover the whole study area, hence we stitch the two RS maps after radiometric calibration and FLAASH into one map that can completely cover the study area. And this function is achieved by the function of SeamlessMosaic in ENVI 5.3. To create the final area map that can be used for the classification that follows, the stitched image is cropped in accordance with the vector boundary of the study area.

### 3.3. RF classification

The RF model is just a classification method that we selected because it has demonstrated greater accuracy than other popular classifiers (Granata *et al.* 2022a, 2022b; Di Nunno *et al.* 2023a, 2023b, 2023c), such as support vector machine (SVM), K-nearest neighbor (KNN), or multi-label classification (MLC), in many applications (Speiser *et al.* 2019). When classifying land cover using RS data, RF is currently regarded as one of the most popular techniques (Millard & Richardson 2015; Li *et al.* 2016; Teluguntla *et al.* 2018; Maxwell *et al.* 2019). The explanations for RF receiving significant enthusiasm over the last two decades are as follows: (1) good performance by the outliers and noisier datasets; (2) good performance with high-dimensional and multi-source datasets; (3) greater accuracy than other popular classifiers as mentioned previously, such as SVM, KNN, or MLC, in many applications (Abdel-Rahman *et al.* 2014; Rodriguez-Galiano & Chica-Rivas 2014); and (4) promoting the processing speed by selecting important variables (Van Beijma *et al.* 2014). Generally speaking, the key advantages of the RF model are as follows: reduced overfitting, improved accuracy by combining the predictions of multiple trees in comparison with single decision trees, handling nonlinearity when dealing with complex datasets, robustness to outliers by averaging of predictions from multiple trees for the reduction of the impact of outliers, feature importance, handling missing values, reduction of bias values by averaging the predictions of many trees with different initializations and training subsets, less hyperparameter tuning, and reduction of variance. In supervised learning, the algorithm learns from a labeled dataset, where the input data are associated with corresponding target labels or outcomes. The goal is to learn a mapping from inputs to outputs, so the algorithm can make predictions on new, unseen data. RF is made up of several classifiers each of which contributes one vote to the most frequent class assignment for the input vector ($x$),

$$\hat{C}_{rf}^{B} = \text{majority vote}\{\hat{c}_b(x)\}^{B} \tag{1}$$

where $\hat{c}_b(x)$ is the prediction value of the $b$th tree.

RF differs significantly from the conventional classification tree due to the specificity provided by the fact that it is a mixture of numerous classifiers. As a result, it should be viewed as a distinct classifier idea. RF creates more diverse trees by combining various training data subsets via bagging or bootstrapping (Breiman 2001), which also modifies the sample distribution of the data used by the model, introduces noise, and improves the model's generalization ability. During this process, a random sample of the original dataset is used in place of the original data in this procedure (i.e., does not remove selected data from the input sample to create the next subset). RF is an ensemble classification technique that employs a tree as its fundamental classifier.

$$\{h(x, \Theta_k), k = 1, \ldots, \} \tag{2}$$

with $x$ being the input vector and $\{\Theta_k\}$ being a random vector that is independently and uniformly distributed (Breiman 2001; Hastie *et al.* 2009). In addition, each tree grows without being pruned. After the tree has completed its growth, only a few variables are generated at random for each node's variables. As a result, certain data may be utilized more than once in training the classifier, while other data may never be utilized. In other words, both the samples and variables used are randomized, and this double randomization process is resistant to overfitting. By being more resistant to subtle changes in the input data, the classifier becomes more stable. Additionally, the classification's accuracy is increased (Breiman 2001).

In this paper, we conducted RF by using ENVI software (Van der Linden *et al.* 2015), and all parameters are set as follows: n_ Estimators = 400; Impurity Function: Gini Index; Minimum impurity threshold = 0; and Minimum number of samples = 1.

### 3.4. Classification accuracy validation

The confusion matrix is a widely accepted evaluation tool in the field of LULC classification that provides a visual representation of the agreement between predicted and actual classifications. By using the confusion matrix, it is possible to offer a quantitative measure of accuracy, providing the ability to compare results with other classifications or previous results (Congalton 1991).

To ensure correctness, the ground truth data were matched to the categorized image. To assess categorization accuracy, the user accuracy (UA) and producer accuracy (PA) were tested. The accuracy of the producer is determined by dividing the total number of correctly categorized pixels. The inaccuracy of misclassified pixels, as well as misclassification into a different class, was recorded. Furthermore, the user's accuracy is a measurement of the individual class acquired from the pixels classified in the same group (Voss & Sugumaran 2008). The confusion matrix produced for UA and PA was used to calculate the total accuracy. UA, PA, and overall accuracy (OA) are described as follows.

UA and PA are two important performance metrics that are derived from the confusion matrix in the evaluation of LULC classification accuracy. UA is the percentage of samples that are correctly categorized by the classifier relative to the actual sample class. It is calculated as the amount of correctly classified samples (i.e. true positives) divided by the total number of samples (i.e. true positives plus false negatives). PA, on the other hand, is defined as the proportion of samples in a particular class that was correctly classified by the classifier. It is calculated as the number of samples that were correctly categorized (i.e. true positives) divided by the total number of samples that were classified as that particular class (i.e. true positives plus false positives).

Both UA and PA are commonly used to evaluate the performance of LULC classification algorithms. However, it is important to note that while UA measures the OA of the classification, PA provides a class-specific evaluation of accuracy.

$$\text{User accuracy (UA)} = \frac{(\text{Number of true positives} + \text{Number of true negatives})}{(\text{Number of true positives} + \text{Number of false negatives})} \times 100 \tag{3}$$

$$\text{Producer accuracy (PA)} = \frac{\text{Number of true positives}}{(\text{Number of true positives} + \text{Number of false positives})} \times 100 \tag{4}$$

where true positives represent the count of pixels that are correctly classified as positive. True negatives denote the quantity of pixels that are accurately classified as negative. False negatives refer to the pixels that are incorrectly classified as negative, but they should have been classified as positive. Additionally, false positives represent the pixels that are incorrectly classified as positive, but they should have been classified as negative. Total pixels refer to the total number of pixels in the image

$$\text{Overall accuracy (OA)} = \frac{\text{Total number of correct classified}}{\text{Total number of pixels}} \times 100 \tag{5}$$

The Kappa coefficient (KC) is an additional metric used to compare training pixels with ground truth data. It measures the extent of agreement beyond chance by comparing the observed agreement between classification results and reference data to the expected agreement. Kappa values range from $+1.0$ to $-1.0$, with values above 0.7 indicating substantial agreement (Hastie *et al.* 2009). A value of zero suggests no correlation in categorization. Typically, the KC is used alongside other metrics such as OA, UA, and PA to offer a comprehensive evaluation.

$$\text{Kappa coefficient (KC)} = \frac{n\sum_{i=1}^{p} x_{ii} - \sum_{i=1}^{p} x_{i0}x_{0i}}{n^2 - \sum_{i=1}^{p} x_{i0}x_{0i}} \tag{6}$$

where $n$ is the total number of pixels; $p$ is the number of classes; $\sum x_{ii}$ is the total number of elements of the confusion matrix; $\sum x_{i0}$ is the sum of row $i$; and $\sum x_{0i}$ is the sum of column $i$.

### 3.5. Method of LULC change

For the analysis of various types of land-use change and to determine its rate, we employed four indicators. These indicators include the net total change area, annual change area, annual change rate, and dynamic degree.

In order to compute the annual change rate ($K_i$) related to land-use type $i$, the following equation is expressed:

$$K_i = \frac{\Delta s_{i,j}}{s_i} \times \frac{1}{t} \times 100\% \tag{7}$$

In the given context, $s_i$ represents the initial area of land-use type $i$ at the beginning of monitoring. $\Delta s_{(i,j)}$ denotes the total net area of changes between land-use types, where $j$ changes to or from land-use type $i$ during the time period $t$. $K_i$ is calculated for the case study over the time period $t$.

Equation (8) is utilized to calculate the dynamic degree ($L$) of $i$:

$$L = \frac{\sum_{i=1}^{n} |s_i - s_j|}{\sum_{i=1}^{n} s_i} \times \frac{1}{t} \times 100\% \tag{8}$$

where $s_i$ represents the area of a specific land type at the start of the study, while $s_j$ represents the area of the same land type at the end of the study. The variable $n$ corresponds to the total number of land types ($n = 1,2,3,\ldots$), and $t$ represents the time duration of the case study.

### 3.6. Land-use transfer matrix

In this research, the areas of six distinct LULC types were utilized to compute the land-use transfer matrices for seven time periods from 1992 to 2022 in Jinan City. The land-use transfer matrix (LUTM) (Van der Linden *et al.* 2015) is an extension of the Markov transfer matrix, initially used to describe transitions from one state to another over a specific period. It has been widely employed in academic literature to gain deeper insights into the evolution of land-use change (Congalton 1991) and is particularly useful in describing the conversions between various land-use types (Voss & Sugumaran 2008). The calculation was performed using ArcGIS 10.2.2, and the LUTM calculation equation is provided as follows:

$$S_{ij} = \begin{bmatrix} s_{11} & s_{12} & \cdots & s_{1n} \\ s_{21} & s_{22} & \cdots & s_{2n} \\ \cdots & \cdots & \cdots & \cdots \\ s_{n1} & s_{n2} & \cdots & s_{nn} \end{bmatrix} \tag{9}$$

where $S_{ij}$ represents the area transformed from land-use type $i$ to land-use type $j$. At the start and the end of the study period, $i$ and $j$ denote the specific land-use type, and $n$ denotes the total number of land-use types. The LUTM (introduced as Equation (9)) is a two-dimensional matrix obtained based on the changes in land-cover status at different times in the same region. By analyzing the obtained transfer matrix, we can obtain the mutual transformation between two different land types in different time periods. It describes the land types that have undergone changes in different years, as well as the location and area of the changes. LUTM reflects not only the static fixed area and time data of the various land types mentioned above but also a more abundant initial area transfer of each land type and the final area transfer of each land type. In most cases, a certain type of land is not simply converted to another land type, but rather to multiple land types.

### 3.7. Driving forces of LULC change

The interaction between human activity and the natural environment leads to land-use change, which is a crucial aspect of regional sustainable development (Van Asselen & Verburg 2013; Ge *et al.* 2019). Human activities have surpassed the constraints imposed by the physical geography of the planet by implementing advanced farming methods and engineering solutions, such as land consolidation, which have changed the geographic distribution and type of regional LULC (Zhou *et al.* 2020). Land-use change is primarily driven by human activities related to urbanization, population rise, and LULC management policies. These factors have indirect effects on LULC (Du *et al.* 2014). The PCA was employed to calculate the

principal component using the following variables: total annual precipitation, mean temperature, GDP, total population, UP, resident population per unit area, urban people's income, farmer income, and fixed asset investment (Table 2). During the period 1992–2022, we collected each dataset on an annual basis for the purposes of pre-processing. SPSS software was utilized to conduct the PCA.

This study introduces a 'two-step' analytical approach. Initially, all identified factors from the general LULC analysis undergo a PCA. In the second step, the key variables are identified within the significant dimensions, and stepwise regression modeling is conducted to assess the interaction between typical LULC and these essential variables.

#### 3.7.1. Principal component analysis

To examine the factors influencing LULC change, we included a range of socioeconomic and natural climate indicators. However, there might be significant correlations (informational overlap) among these various indicators. To address this issue, we initially filtered the variables using PCA.

PCA is a multivariate statistical technique used to assess the level of correlation among different variables. It replaces the initial variables with a new set of composite variables that are uncorrelated by combining multiple variables with specific correlations. The primary goal is to retain as much information as possible while reducing the dimensionality of the variable dataset. This is achieved by orthogonally transforming a set of potentially correlated variables into a new set of linearly independent variables, with the top few variables retaining the majority of the variance present in the original variables (Li *et al.* 2021). These transformed variables are referred to as principal components and are used in subsequent analyses.

In mathematical terms, let us assume that there are $n$ samples of $x$, and each sample consists of $p$ variables. We can represent this as a matrix of dimensions $n \times p$.

$$X = \begin{bmatrix} x_{11} & x_{12} & \dots & x_{1p} \\ x_{21} & x_{22} & \dots & x_{2p} \\ \dots & \dots & \dots & \dots \\ x_{n1} & x_{n2} & \dots & x_{np} \end{bmatrix} \tag{10}$$

These comprehensive indices were obtained by applying a linear transformation to this variable, respectively: $z_1$, $z_2$,…, $z_m$ ($m \leq p$)

$$\begin{cases} z_1 = l_{11}x_1 + l_{12}x_2 + \dots + l_{1p}x_p \\ z_2 = l_{21}x_1 + l_{22}x_2 + \dots + l_{2p}x_p \\ \dots \\ z_m = l_{m1}x_1 + l_{m2}x_2 + \dots + l_{mp}x_p \end{cases} \tag{11}$$

In this equation, the coefficient $l_{ij}$ is defined with the aid of two main principles: (i) $z_i$ is not influenced by $z_j$ and (ii) $z_1$ exhibits the highest variance among all linear combinations, while $z_m$ displays the lowest variance. The new variables (i.e., $z_1$, $z_2$, and $z_3$) represent the first, second, and third principal components of the original variables. In practical applications, to simplify the relationship between variables, the top few principal components with the highest variances are often utilized.

### 3.8. Multiple linear regression analysis

The multiple stepwise technique is a regression model fitting method that involves an automated procedure to repeatedly perform regression analysis and significance testing on explanatory variables. Only those variables that significantly contribute to improving the model are ultimately retained. This is accomplished by evaluating a group of explanatory factors for addition or deletion in accordance with some predetermined criteria. The following is the multiple regression model:

$$Y = \beta + \alpha_1 X_1 + \alpha_2 X_2 + \dots + \alpha_n X_n \tag{12}$$

where $\alpha_1$, $\alpha_2$, … , $\alpha_n$ denote the weighting coefficients, and $\beta$ is introduced as a bias/constant term. This research used SPSS software to implement PCA and the multiple linear regression analysis.

### 3.9. Classification accuracy

The reliability of the classification results is shown by the accuracy of the classification. The OA is more than 90%, and the Kappa value is more than 85. Thus, the accuracy results show that the results of the classification are highly reliable (Table 4).

**Table 4** | LULC/land cover classification accuracy from 1992 to 2022

| Classification category | User accuracy | Producers' accuracy |
|---|---|---|
| Impervious surfaces | [84.85%, 96.43%] | [97.91%, 100%] |
| Water bodies | [99.15%, 100%] | [84.31%, 98.59%] |
| Farmland | [66.41%, 99.42%] | [86.99%, 100%] |
| Woodland | [80.57%, 99.17%] | [91.26%, 99.97%] |
| Bare land | [74.48%, 100%] | [20%, 100%] |
| OA | [90.7561%, 95.1314%] | KC [0.8686, 0.9141] |

### 3.10. Quantity and spatial distribution of LULC

Over the past three decades, there have been substantial changes in the LULC of Jinan City. Notably, there has been a significant increase in the impervious surface area, while the area of bare land has decreased, as can be determined from Table 5 and the spatial distribution map (Figure 3). The area of bare land has experienced fluctuations, initially increasing and then decreasing, resulting in an overall area decrease. The farmland also experienced fluctuations, while the total area remained stable during 30 years. The overall area of the water body remained stable and almost unchanged; the Woodland shows a slight downward trend. In addition, the average rate of change over these 30 years was ordered as impervious surface > bare land > water > woodland > farmland.

For these six time periods, their dynamic degree is ranked as 2002–2006 > 1998–2002 > 2017–2022 > 1992–1998 > 2006–2011 > 2011–2017 (Table 6). Among them, the dynamic degree is the highest in 2002–2006 (7.35%), indicating that the changes in various types of LULC are the greatest during this time period, and the degree of change in bare land is significant (−74%), which may be due to the government's vigorous construction of houses or factories on bare land during this period of accelerated urbanization. On the contrary, the period from 2011 to 2017 showed the least dynamic attitude (0.32%), indicating that there was little change in the various LULC types during this period.

The area of impervious surfaces showed a sharp and upward trend between 1992 and 2022 (Table 5 and Figure 4). In 1992, the area of impervious surfaces only accounted for 2,348 $km^2$, and it rose to 4,795 $km^2$ in 2022. This increase is likely due to the rapid urbanization and economic development in the region, which has led to an increase in the demand for land for commercial and residential purposes. To compensate for this expansion, the areas of bare land and woodland reduced by 1,800 and 686 $km^2$, respectively. In 1992, impervious surfaces mainly occupied two districts (Lixia District and Shizhong District, about 36°40′N, 117°E), which have continuously expanded over the past 30 years. In 2022, this area almost span the entire central administrative region (Huaiying District, Shizhong District, Lixia District, Licheng District, and Zhangqiu District). The construction area of Laiwu District and Gangcheng District, which are located in the southeast direction, has continuously expanded, forming the second largest impervious surface area except for the central area.

**Table 5** | Area for each type of LULC/land cover

| Area for each type of LULC/land cover($km^2$) | | | | | | | |
|---|---|---|---|---|---|---|---|
| | Research year | | | | | | |
| Classification Category | 1992 | 1998 | 2002 | 2006 | 2011 | 2017 | 2022 |
| Impervious surfaces | 2,348.85 | 2,663.99 | 2,959.29 | 3,465.73 | 3,671.33 | 4,059.49 | 4,795.35 |
| Water bodies | 81.36 | 90.89 | 77.00 | 121.05 | 89.32 | 117.87 | 127.40 |
| Farmland | 2,109.92 | 2,401.25 | 1,933.30 | 2,883.48 | 2,812.43 | 2,562.78 | 2,103.97 |
| Woodland | 3,774.52 | 3,861.84 | 3,587.98 | 3,314.91 | 3,083.91 | 3,043.83 | 3,088.28 |
| Bare land | 1,888.05 | 1,184.74 | 1,645.15 | 421.11 | 550.10 | 422.30 | 91.29 |
| Total | 10,202.71 | 10,202.71 | 10,202.71 | 10,206.28 | 10,207.09 | 10,206.27 | 10,206.28 |

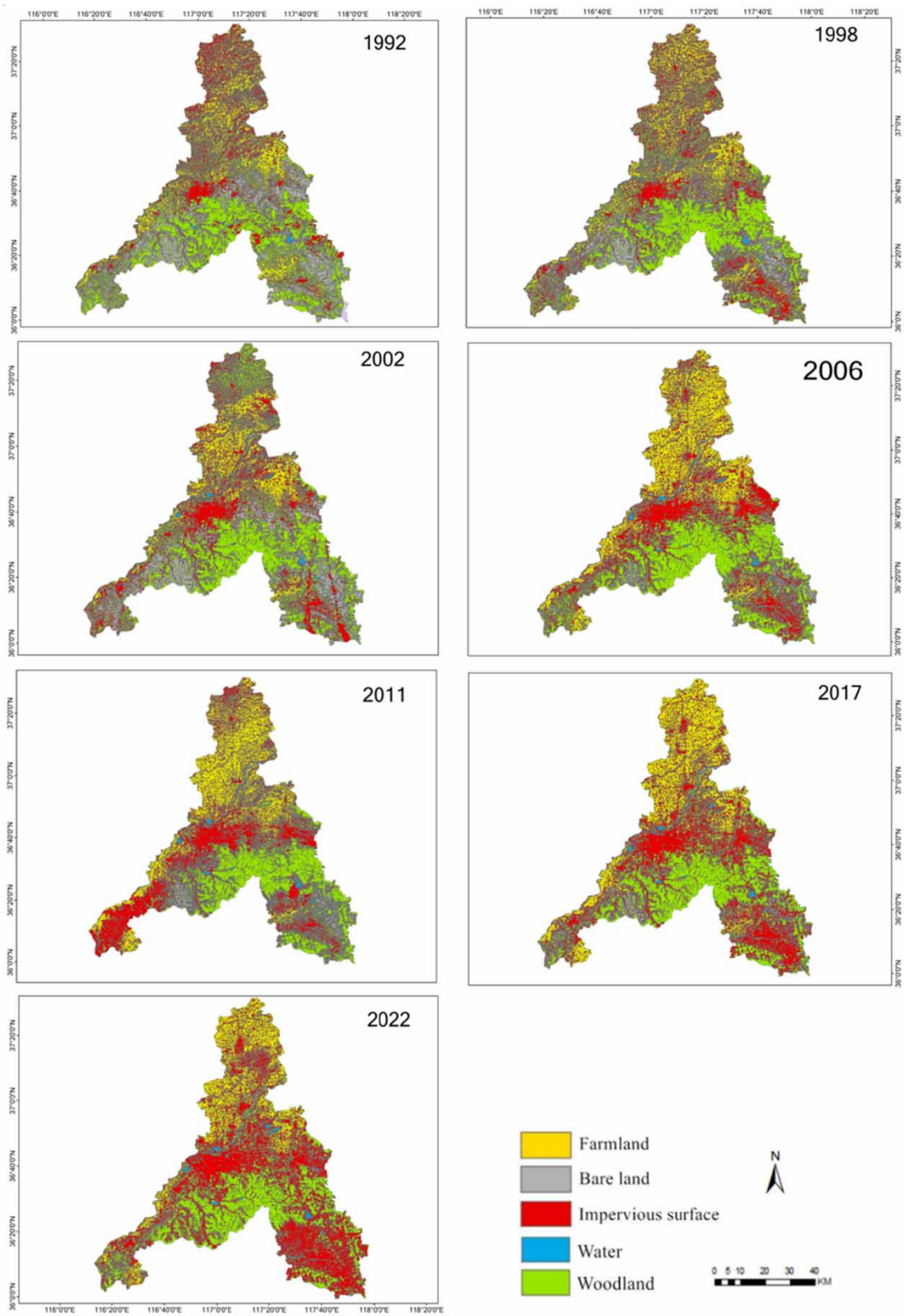


**Figure 3** | Land-use maps of Jinan province in the reference years.

**Table 6** | LULC factors of change in the reference years

| Research year | Factors of change | Impervious surfaces | Water bodies | Farmland | Woodland | Bare land |
|---|---|---|---|---|---|---|
| 1992–1998 | Amount ($km^2$) | 315.14 | 9.53 | 291.33 | 87.32 | − 703.31 |
| | Rate ($km^2$/year) | 52.52 | 1.59 | 48.55 | 14.55 | − 117.22 |
| | $K_i$ | 13.42% | 11.71% | 13.81% | 2.31% | − 37.25% |
| | $L$ | | | 2.30% | | |
| 1998–2002 | Amount ($km^2$) | 295.29 | − 13.89 | − 467.95 | − 273.86 | 460.41 |
| | Rate ($km^2$/year) | 73.82 | − 3.47 | − 116.99 | − 68.47 | 115.10 |
| | $K_i$ | 11.08% | − 3.82% | − 19.49% | − 7.09% | 38.86% |
| | $L$ | | | 3.70% | | |
| 2002–2006 | Amount ($km^2$) | 506.45 | 44.06 | 950.18 | − 273.07 | − 1,227.61 |
| | Rate ($km^2$/year) | 126.61 | 11.01 | 237.54 | − 68.27 | − 306.90 |
| | $K_i$ | 17.11% | 57.22% | 49.15% | − 7.61% | − 74.62% |
| | $L$ | | | 7.35% | | |
| 2006–2011 | Amount ($km^2$) | 205.59 | − 31.73 | − 71.05 | − 231.00 | 128.18 |
| | Rate ($km^2$/year) | 41.12 | − 6.35 | − 14.21 | − 46.20 | 25.64 |
| | $K_i$ | 5.93% | − 26.21% | − 2.46% | − 6.97% | 30.70% |
| | $L$ | | | 1.90% | | |
| 2011–2017 | Amount ($km^2$) | 388.17 | 28.55 | − 249.65 | − 40.09 | − 126.98 |
| | Rate ($km^2$/year) | 64.69 | 4.76 | − 41.61 | − 6.68 | − 21.16 |
| | $K_i$ | 10.57% | 31.96% | − 8.88% | − 1.30% | − 23.27% |
| | $L$ | | | 0.32% | | |
| 2017–2022 | Amount ($km^2$) | 735.85 | 9.53 | − 458.82 | 44.45 | − 331.02 |
| | Rate ($km^2$/year) | 147.17 | 1.91 | − 91.76 | 8.89 | − 66.20 |
| | $K_i$ | 18.13% | 1.62% | − 17.90% | 1.46% | − 79.05% |
| | $L$ | | | 3.10% | | |

During the study period, 45.63 $km^2$ of water area was converted to other uses, primarily forest, construction, and agricultural land. Conversely, 91.67 $km^2$ of water surface was created primarily from impervious surface, including a large lake, a network of channels and dams, serving various urban development and water management purposes. Consequently, despite fluctuations over time, the water surface area grew from 81.36 $km^2$ in 1992 to 127.40 $km^2$ in 2022, with a mean that has always been relatively small at approximately 100 $km^2$ (Table 5).

The evolution of bare land area within the studied region reveals a nuanced landscape transformation. In 1992, the expanse of bare land covered 1,888.05 $km^2$, signifying a substantial portion of the terrain. By 1998, this area witnessed a reduction to 1,184.74 $km^2$, hinting at shifts in land use or possible natural vegetation regrowth. Notably, in 2002, the bare land area increased to 1,645.15 $km^2$, suggesting land cover adjustments. However, a pivotal transformation occurred in 2006 when the bare land area dramatically plummeted to a mere 421.11 $km^2$. This substantial decrease may be attributed to urban development, reforestation, or alternative land utilization strategies. By 2011, the bare land area showed a slight increase, reaching 550.10 $km^2$, implying continued land-use changes. In 2017, the area experienced a modest reduction, lowering it to 422.30 $km^2$, and it continuously decreased to 91.29 $km^2$ in 2022. This pronounced reduction likely reflects substantial shifts in land use, possibly driven by urbanization, agricultural expansion, or deliberate afforestation efforts.

There was a fluctuation trend in woodland over the last 30 years (Figure 4). The area grew from 1992 to 1998, and it decreased slowly from 1998 to 2011 to achieve a stable line until 2022. Over the past 30 years, the total woodland area that was converted to other types of land was 686 $km^2$, mainly for impervious surfaces. Therefore, from accounting for the biggest part of about 37% of the total area in 1992, Jinan province had approximately 30% area in 2022 (Table 5). This decline is most likely caused by the growth of urban areas, the creation of infrastructure, and the commercial exploitation of forests. However, over the past 30 years, the primary spatial distribution of woodland in Jinan City has remained largely unchanged. The majority of woodland is concentrated in the southern parts of the Changqing, Licheng, Zhangqiu, and Laiwu Districts. Further investigation revealed that the southern region is predominantly mountainous, with forested areas covering a significant portion of the landscape.

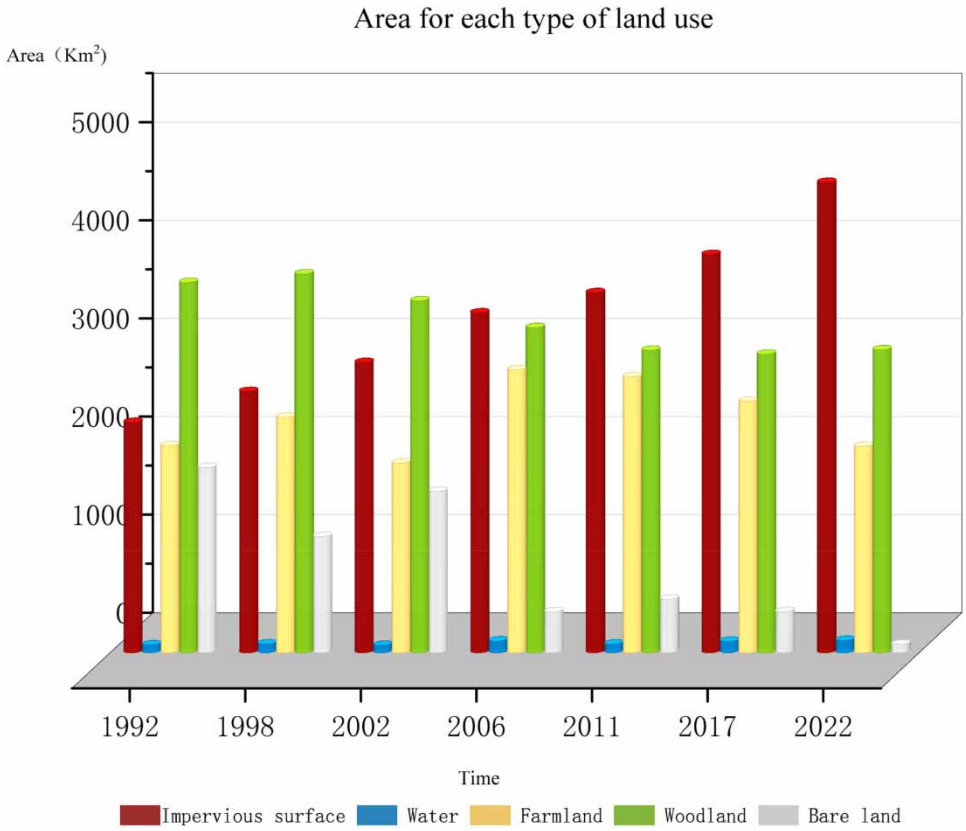


**Figure 4** | The areas of different types of LULC from 1992 to 2022.

Unlike the abovementioned types of land, farmland experienced growth as well as decline, and fluctuated over the last 30 years (Figure 4). But the area between the beginning and the end of the studied period was almost the same, changing from 2,110 to 2,104 $km^2$, respectively, with a maximum in 2006–2011 of around 2,800–2,900 $km^2$. The majority of the cultivated land in Jinan City is concentrated in the northern region, where it is interspersed with clusters of impervious surfaces. While the patch-like areas of cultivated land have gradually expanded over time, the distribution remains primarily focused in the northern area.

### 3.11. LULC transition characteristics

The LULC transfer matrix of Jinan City was obtained by comparing the results of LULC classification in seven different periods using ENVI software, as shown in Table 6 and Figure 5. Over the past 30 years, all types of land have transformed.

Between 1992 and 1998, approximately 14% of the woodland had been converted to other land types, such as impervious surfaces, farmland, and bare land (Table 7). Some parts of the bare land were transformed into impervious surfaces and woodland, while farmland was mainly converted to woodland and impervious surfaces. During this period, the area of concessions for bare land was lower than the area of transfers, amounting to approximately 700 $km^2$, while the area of concessions for other types of land was higher than the area of transfers. In particular, both farmland and impervious surface areas increased by approximately 13%.

Between 2002 and 2006, the largest gap between inward and outward transfers occurred for bare land, resulting in a decrease of approximately 12% in its area. Farmland, impervious surfaces, and water were converted into each other, and the transfer volume for these three land types was higher than the transfer out. By contrast, the transfer volume for woodland was lower than the transfer out, with most of it being converted to impervious surfaces. As a result, the area of bare land and woodland decreased during this period, with a portion of the reduction being transformed into the other three land types.

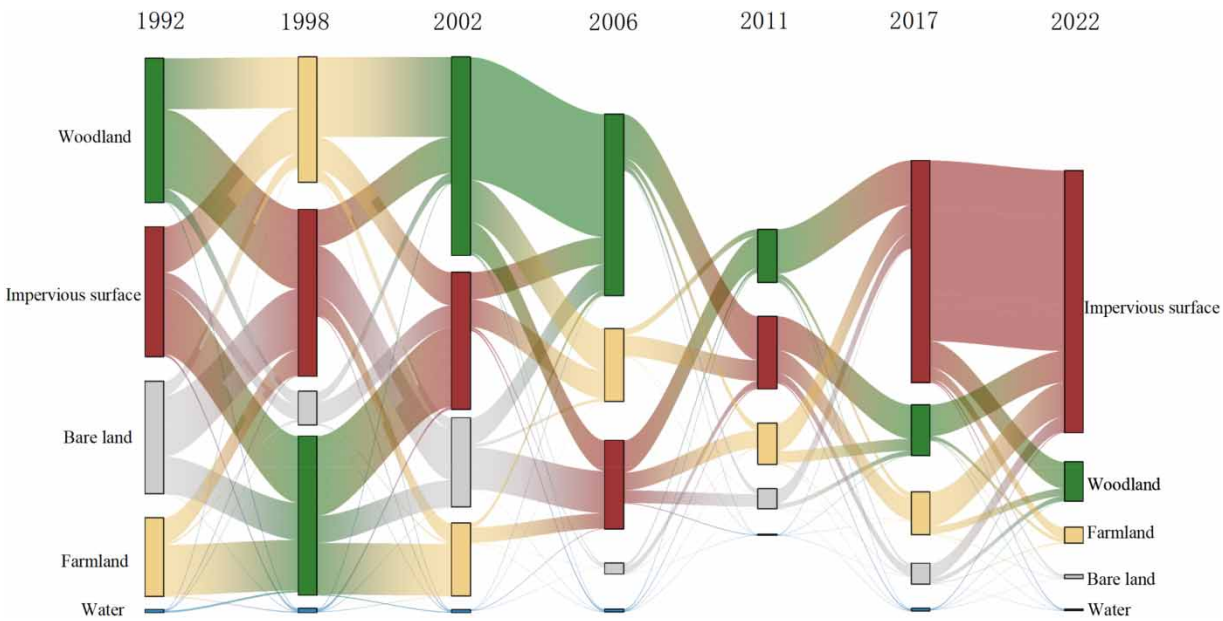


**Figure 5** | Sankey diagram of the LULC transfer matrix.

During the three time periods of 2006–2011, 2011–2017, and 2017–2022, the area of land transfer for all types was less, except for the increase of impervious surfaces in the last period. The transfer area of impervious surfaces exceeded the transfer out area, resulting in an 18% increase in their total area between 2017 and 2022. During these three time periods, the total area of impervious surfaces increased, while the areas of farmland decreased. These types of land were converted into each other, with the Sankey diagram indicating that the transfer area for various types of land during the 2006–2017 period was lower than that of the other research periods.

### 3.12. Driving force of LULC

#### 3.12.1. Economic and population development

We used nine factors, such as GDP and population, as input data for the 30 consecutive years from 1992 to 2022, in other words, 9 * 30 sets of data were used as raw data for PCA input. Afterward, all data were standardized in SPSS, followed by the Kaiser–Meyer–Olkin (KMO) and Bartlett tests. The results of this experiment were KMO = 0.775 > 0.5 and $P < 0.05$. Therefore, it was concluded that these 30 sets of data have structural validity and can be used for PCA.

Using PCA, each of the nine indicators' change data could be reduced to two components (Table 8). The first principal component (F1) is a description of economic growth, reflecting primarily the changes in the GDP (X1), UI (X5), FI (X6), PP (X2), UP (X3), and POD (X4). The second principal component (F2) primarily reflects AT (X8) and AR (X9) to characterize regional climate change.

Multiple linear regression analysis (Table 9) could be used to derive the statistical model of the relationship between the changes in the land area and the primary driving factors. The significance test was passed by the driving relationship models of every kind of land. The particular models demonstrated the following.

This reflects the previous expansion of construction areas, which occurred concurrently with the swift growth of the national economy and the consistent acceleration of Jinan's population growth.

Water area exhibited a negative (reverse) correlation with economic factors (F1) and a positive correlation with climate factors (F2), with F1 having the most significant influence; however, it is not significant, nor is it significant for farmland. Therefore, we will not discuss it.

Some traditional water bodies are near urban and rural construction sites, although their impact is not expected to be substantial. Conversely, climate change-related factors, such as increased precipitation, will likely result in denser water bodies in Jinan. Farmland areas had a negative correlation with the economy (F1) and a positive correlation with climate (F2). It was influenced primarily by economic expansion. The woodland area had a positive correlation with climate change and a

**Table 7** | LULC transition matrix for 1992–2022

| | 1998 | | | | | |
|---|---|---|---|---|---|---|
| **1992** | **Bare land** | **Impervious surface** | **Farmland** | **Water** | **Woodland** | **Total** |
| Bare land | 8.38% | 1.36% | 0.18% | 0.00% | 1.17% | 11.10% |
| Impervious surfaces | 5.48% | 11.45% | 2.27% | 0.08% | 7.13% | 26.40% |
| Farmland | 1.27% | 4.10% | 13.19% | 0.03% | 4.57% | 23.11% |
| Water bodies | 0.00% | 0.23% | 0.10% | 0.52% | 0.06% | 0.88% |
| Woodland | 3.32% | 5.97% | 4.54% | 0.17% | 24.44% | 38.39% |
| Total | 18.46% | 23.10% | 20.27% | 0.79% | 37.38% | 100.00% |
| 1998 | 2002 | | | | | |
| Bare land | 8.12% | 4.53% | 1.04% | 0.00% | 2.42% | 16.11% |
| Impervious surfaces | 1.96% | 16.79% | 2.98% | 0.24% | 7.15% | 29.11% |
| Farmland | 0.16% | 1.72% | 11.88% | 0.05% | 4.63% | 18.42% |
| Water bodies | 0.00% | 0.13% | 0.05% | 0.54% | 0.08% | 0.80% |
| Woodland | 0.90% | 3.25% | 7.17% | 0.05% | 24.19% | 35.55% |
| Total | 11.14% | 26.41% | 23.11% | 0.88% | 38.46% | 100.00% |
| 2006 | 2002 | | | | | |
| Bare/low-cover land | 3.26% | 0.40% | 0.06% | 0.00% | 0.34% | 4.07% |
| Impervious surfaces | 7.56% | 18.51% | 2.72% | 0.12% | 5.50% | 34.42% |
| Farmland | 0.51% | 4.95% | 14.78% | 0.03% | 7.57% | 27.84% |
| Water bodies | 0.03% | 0.37% | 0.05% | 0.63% | 0.08% | 1.15% |
| Woodland | 4.76% | 4.88% | 0.81% | 0.02% | 22.06% | 32.52% |
| Total | 16.11% | 29.11% | 18.42% | 0.80% | 35.55% | 100.00% |
| 2006 | 2011 | | | | | |
| Bare land | 2.07% | 2.26% | 0.05% | 0.01% | 0.94% | 5.33% |
| Impervious surfaces | 1.22% | 23.07% | 3.74% | 0.20% | 7.89% | 36.12% |
| Farmland | 0.11% | 3.17% | 22.84% | 0.02% | 1.30% | 27.45% |
| Water bodies | 0.00% | 0.14% | 0.01% | 0.69% | 0.04% | 0.88% |
| Woodland | 0.66% | 5.78% | 1.20% | 0.22% | 22.34% | 30.22% |
| Total | 4.07% | 34.42% | 27.84% | 1.15% | 32.52% | 100.00% |
| 2017 | 2011 | | | | | |
| Bare land | 1.67% | 1.64% | 0.17% | 0.00% | 0.52% | 4.01% |
| Impervious surfaces | 2.71% | 24.03% | 5.03% | 0.13% | 7.96% | 39.87% |
| Farmland | 0.06% | 4.07% | 20.06% | 0.01% | 0.94% | 25.14% |
| Water bodies | 0.02% | 0.26% | 0.05% | 0.72% | 0.12% | 1.15% |
| Woodland | 0.87% | 6.13% | 2.14% | 0.02% | 20.67% | 29.84% |
| Total | 5.33% | 36.12% | 27.45% | 0.88% | 30.22% | 100.00% |
| 2022 | 2017 | | | | | |
| Bare land | 0.29% | 0.44% | 0.13% | 0.00% | 0.12% | 0.97% |
| Impervious surfaces | 2.68% | 32.41% | 6.12% | 0.21% | 5.64% | 47.06% |
| Farmland | 0.17% | 1.99% | 17.50% | 0.01% | 0.66% | 20.33% |
| Water bodies | 0.00% | 0.24% | 0.03% | 0.92% | 0.06% | 1.24% |
| Woodland | 0.87% | 4.79% | 1.36% | 0.02% | 23.36% | 30.39% |
| Total | 4.01% | 39.87% | 25.14% | 1.15% | 29.84% | 100.00% |

**Table 8** | Component matrix of the PCA in this research

| Factors | Variables | Component | |
|---|---|---|---|
| | | F1 | F2 |
| GDP | X1 | 0.963 | 0.119 |
| PP | X2 | 0.905 | 0.071 |
| UP | X3 | 0.979 | 0.074 |
| POD | X4 | 0.986 | −0.048 |
| Urban Income (UI) | X5 | 0.987 | −0.048 |
| Farmers Income (FI) | X6 | 0.981 | −0.073 |
| Fixed Assets Investment (FAI) | X7 | 0.979 | −0.067 |
| AT | X8 | 0.039 | −0.766 |
| AR | X9 | 0.015 | 0.795 |

**Table 9** | Linear relationships between land change and PCA for various types of land

| Impervious surfaces | Water bodies | Farmland | Woodland | Bare land |
|---|---|---|---|---|
| $Y = 3{,}206.72 + 541.040 * F1$ $R^2 = 0.748, P < 0.05$ | $Y = 95.99 - 9.16 * F1 + 0.9 * F2$ $R^2 = 0.013, P > 0.05$ | $Y = 2{,}482.23 - 198.40 * F1 + 41.527 * F1$ $R^2 = 0.046, P > 0.05$ | $Y = 3{,}438.612 - 2.99 * F1 + 50.61 * F2$ $R^2 = 0.577, P < 0.05$ | $Y = 979.17 - 452.60 * F1 - 57.26 * F2$ $R^2 = 0.660, P < 0.05$ |

negative correlation with the economy (F1). This is a result of the traditional woodland being encroached upon by urban development and impervious surface expansion, but this encroachment is not a significant factor. However, the expansion of woodlands will be brought on by climate change, particularly the increase in precipitation. The area of bare land exhibited a negative correlation with both the economy (F1) and climate change (F2), with F1 being the primary influencing factor. This suggests that the development of construction or urban expansion utilized the bare land area, resulting in significant development for construction purposes.

### 3.12.2. Government policies

LULC change can be considerably influenced by government planning and industrial development policies. China's population of 1.4 billion people faces significant food security and environmental challenges. The government has to encourage economic growth, enhance the quality of life, and protect the environment. During periods of rapid economic expansion and increasing population (Figure 6), housing, transportation, and industry will require more land. Large tracts of farmland and undeveloped land have been occupied, while the amount of land devoted to construction has risen sharply (Figure 4). During the period between 1992 and 2005, the rate of development in Jinan was relatively slow, resulting in a significant disparity between the municipal districts and other cities. Thus, the area of the impervious surfaces grew swiftly in the municipal districts (Figure 3 and Table 5), while it grew slowly in the remaining regions. The construction of Harmonious Jinan (COHJ) was established in 2005. This city was included in both the 'Eleventh Five-Year' plan and the national development strategy. The COHJ become a master plan for development and boosting the economy. Since 2015, Jinan has identified 'building four centers' as the core strategic goal of its construction and development, clearly proposing to make Jinan an important regional scientific and technological innovation center in the country. In addition, the 'Three-Year Plan' clearly proposed to accelerate the interconnection of transportation facilities, strengthen regional ties and cooperation, and jointly build the 'The Belt and Road' land. These policies promote industrial cooperation among cities along the Yellow River and jointly build demonstration belts for industrial cooperation, which will result in rapid development for the industrial and construction industries.

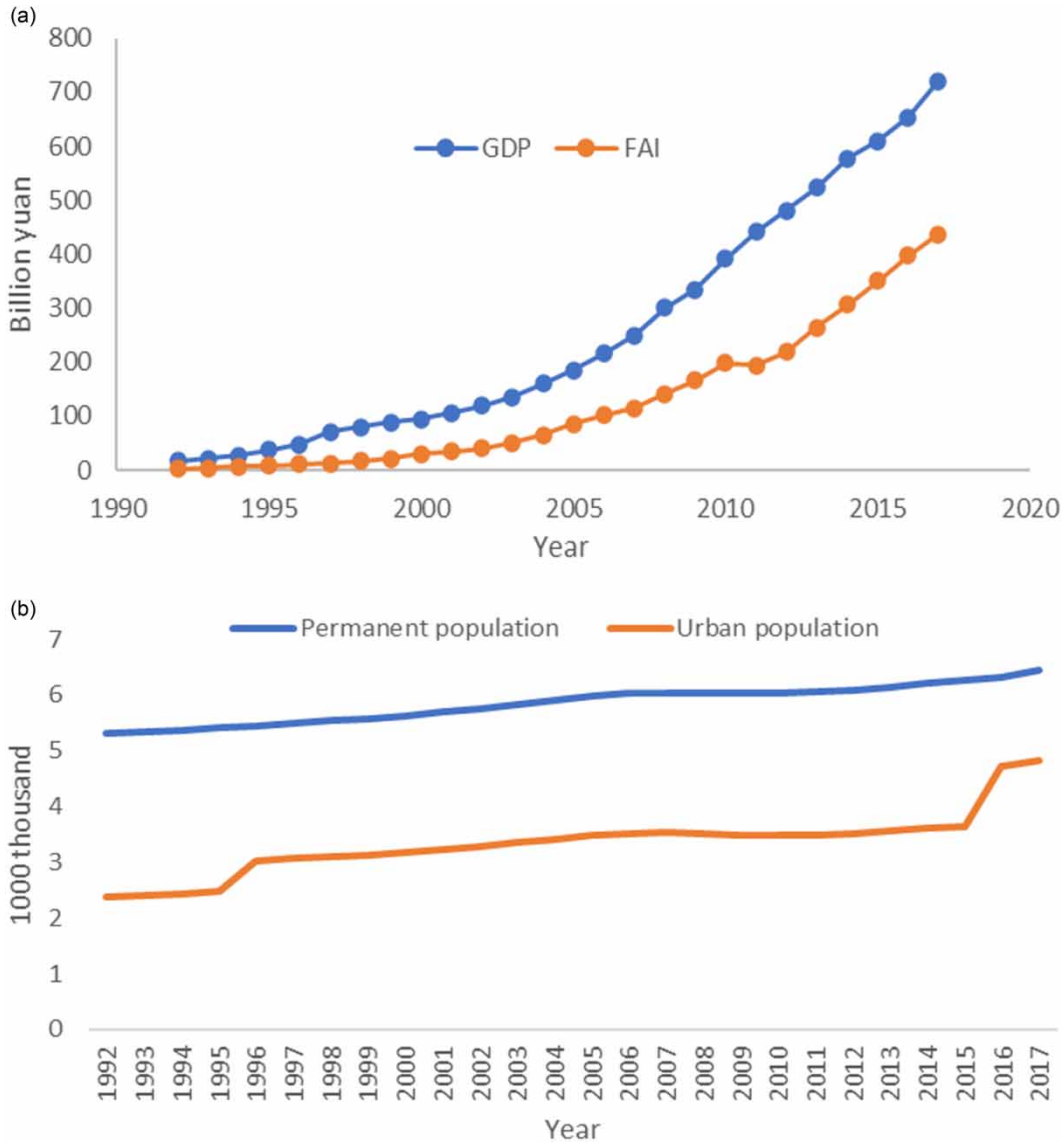


**Figure 6** | Variations of (a) economic factors and (b) populations in Jinan during 1992–2017. *Note*: GDP, gross domestic product and FAI, fixed assets investment.

The traditional planning concept for Jinan's 'central urban area' has been replaced with 'main city'. The eastern urban area, western urban area, and old urban area are named Dongcheng, Xicheng, and Zhongcheng, respectively. As a consequence, regional development primarily occurred in centralized areas, leading to the expansion of developed land in the connecting zones. These changes illustrate the significant impact of policies on regional LULC modifications. The expansion of developed land has resulted in a significant loss of bare land, which is now the largest of the four types of land resources.

China has implemented several initiatives to preserve agricultural land to ensure food security. The most well-known program is the 'Basic Farmland Protection System,' which ensures China has at least 1.2 million $km^2$ of essential farmland available for agriculture and the nation's total food self-sufficiency. The alternative strategy, known as the 'Balance of Arable Land' policy, requires that any conversion of arable land must be offset by the acquisition of land elsewhere. These land policies have postponed the loss of arable land. In the current study, we found that between 1992 and 2022, a sizeable percentage of impervious surfaces was converted into farmland (Tables 5 and 6). This finding is in line with other researchers'

findings and may be explained by the terrain. Because Jinan is a plain region, it is more practical to convert developed land to farmland. This was significantly dissimilar from other areas, such as Nairobi, Kenya, and the Bale Mountains, Ethiopia, where farmland was primarily created by clearing existing vegetation (Du *et al.* 2014). Unused land should be carefully utilized, considering it is a vital resource for the land reserve (Li *et al.* 2021). In urban growth, it is crucial to regulate the construction of new structures on farmed and unused land. Both the quantity and the quality of farmland should not be impacted, and the balance of farmed land must be properly managed.

In terms of sustainable LULC management, Jinan will assume a greater number of economic development responsibilities, thereby introducing new challenges. This study indicates that the main obstacles affecting the sustainable utilization of land resources in Jinan are the rapid increase in impermeable water surface and the reduction of woodland (Figure 4). Moreover, the economy (UP and GDP) and climate change were the primary drivers of LULC change (Tables 7 and 8). Therefore, departments tasked with the sustainable management of Jinan should prioritize the reasonable utilization of various types of impervious surfaces. Some new construction projects should first utilize existing impervious surfaces, strictly control new land, fully utilize unused land, and minimize the occupation of arable land. Furthermore, departments ought to regulate UP growth and guarantee an appropriate range of GDP increase to enhance the use efficiency of impervious surfaces and the level of sustainable LULC. The policies of the government have a significant impact on regional LULC. The implementation of sustainable LULC policies by land management departments in Jinan will promote the effective utilization and long-term growth of regional land as well as enhance the level of regional land management.

Future studies could use the data on LULC quantity and spatial distribution as the foundation for assessing Jinan's LULC sustainability. To evaluate the spatial variation in sustainable LULC in Jinan, the level of sustainable LULC will be determined. This will allow departments of land management to continue to develop their regional sustainable LULC policies.

## 4. DISCUSSION

This study employed RS imagery, GIS, and socioeconomic data to quantitatively assess LULC changes and distributions in Jinan City from 1992 to 2022 (Figure 3). The findings highlight substantial urban expansion, with impervious surfaces more than doubling while bare land decreased significantly (Table 5). Farmland predominantly clustered in the north, while woodland, located primarily in the south, decreased over time. The analysis shows water bodies undergoing conversions and expansions in the past three decades, with new surfaces such as lakes, channels, and dams primarily originating from impervious areas to aid urban development and water management. However, these changes in water areas have been relatively minor compared with the shifts in other land cover types. The main driving forces behind these changes encompass economic development, population growth, and climate variability (Table 8). Notably, qualitative assessments indicate that government policies, notably the 'Construction of Harmonious Jinan,' exerted a noteworthy influence on LULC changes. Consequently, this research underscores the imperative for ecologically sound policies and sustainable urban planning to mitigate adverse environmental consequences. This study employed methods such as supervised classification, PCA, and regression analysis, to construct a spatial database of evaluation factors based on seven time periods from 1992 to 2022.

This study aligns harmoniously with the existing body of literature that has diligently examined the intricate facets of LULC transformations and the underlying forces propelling them. The judicious amalgamation of RS imagery, GISs, and socioeconomic data in deciphering the nuanced dynamics and conversions of LULC in response to urbanization reflects a methodological continuity with analogous investigations conducted in various regions across China (Tian *et al.* 2014). In congruence with prior research, the findings of this study underscore the pivotal roles played by economic development, burgeoning population, and the strategic influence of government policies as primary drivers of LULC alterations (Wulder *et al.* 2008). However, it is imperative to underscore the unique contribution of this study, which distinguishes itself by offering an intricate dissection of LULC transitions specifically within Jinan City. This contribution is marked by its meticulous delineation of spatial patterns, the precise quantification of change magnitude, and the resounding emphasis on the exigency of ecologically sensitive policies and sustainable urban planning, thereby enriching the scholarly discourse in this domain.

Compared with previous land-use studies, our approach exhibits notable distinctions in several pivotal aspects. Conventional supervised classification methods are conventionally utilized for land-use change classification, relying on prior knowledge and sample training, yet they are vulnerable to the intricacies and noise inherent in RS data. By contrast, we have opted for

the RF classification method, a machine learning technique renowned for its adeptness in handling large-scale RS data (Abdel-Rahman *et al.* 2014; Rodriguez-Galiano & Chica-Rivas 2014; Tian *et al.* 2014). The RF method affords us the capability to glean intricate patterns and correlations from the data, consequently facilitating a more precise identification of the driving forces behind land-use changes. Furthermore, we have applied PCA to pinpoint the principal influencing factors (Jolliffe & Cadima 2016), then used multiple linear regression to explore the mechanisms by which these influencing factors affect different types of LULC. The implementation of this amalgamated methodology augments our holistic comprehension of the mechanisms governing land-use changes. Our study shares similarities with the research conducted by Yao *et al.* (2021), as they also employed a similar theoretical framework. However, our study delves deeper within this framework to conduct a more in-depth analysis of the relative importance of different factors, particularly with the support of PCA analysis, to ascertain which factors hold greater influence in different time periods. This comparison highlights that our research offers a more detailed and specific understanding of the driving mechanisms behind land-use change, further enriching the application of the theoretical framework.

This study harnesses data derived from RS imagery, GISs, and socioeconomic factors. However, it is important to acknowledge inherent data limitations regarding accuracy. Notably, the selected study period spans three decades, from 1992 to 2022, potentially overlooking the intricate subtleties and fluctuations in LULC changes that could manifest over shorter time intervals. Within this chosen timeframe, certain finer-grained temporal dynamics may not have received exhaustive scrutiny. Additionally, this study falls short in conducting a comprehensive exploration of the specific environmental impacts and ecological repercussions stemming from the observed LULC alterations. A more extensive analytical approach, encompassing the assessment of effects on biodiversity, ecosystem services, and hydrological systems, could provide a more profound comprehension of the multifaceted environmental implications at hand. In the future, there is potential for advancements in RS data accuracy and resolution, allowing for a more refined observation of land-change trends over shorter time intervals. Emphasis will be placed on investigating the precise impacts of LULC changes on ecosystems. These multifaceted approaches aim to deepen our comprehension of the environmental repercussions stemming from LULC changes, thereby providing invaluable support for sustainable environmental management and policy development.

## 5. CONCLUSION

The availability of information regarding spatio-temporal land-use variation and city development status is crucial for effective land-use projection and decision-making. However, in many urban districts, such as the city of Jinan, such data are often limited. In this study, LULC maps were derived from multi-temporal Landsat images, and spatial analysis techniques and statistical analysis were employed to analyze the spatial–temporal patterns of land-use variation and the driving forces in Jinan from 1992 to 2022.

The study findings revealed diverse trends in the changes of LULC types, with significant transitions observed from bare land and woodland to other types, particularly an increase in impervious surfaces over the course of 30 years. From the present research, it can be concluded that the impervious surfaces of Jinan expanded more than two times than previously. The expansion rates were high and expanded from being concentrated only in two districts to being significantly displayed in each district. Farmland and woodland were located in the northern and southern parts, respectively, and farmland experienced fluctuations while still staying stable in 2022 compared with 1992. The factors affecting the LULC change in Jinan were also discussed. The factors comprise the social economy (GDP and population) and climate. The economy accounts for the main influencing factor in LULC changes.

Urban income, POD, and climate change are the primary drivers of the increase in developed land. Population agglomeration is substantially affected by LULC patterns. When developing LULC policies, the Department of Land Management ought to take into account rationally planning land resources to avoid excessive population concentration. When the Department develops land development tactics, it is critical for it to concentrate on areas experiencing rapid LULC changes. To ensure adequate reserve land, the Department should, if necessary, limit the rate of LULC transfer in an area of volatile LULC change. In response to national low-carbon policies and to reduce harmful gas emissions, attention should also be paid to the climate-influencing factors of urban areas. Further studies on these issues are required. For example, issues such as the urban heat island effect, carbon emissions from impermeable surfaces, and the coupling relationship between urban land change and urban development can provide a basis and reference for sustainable urban development from a more comprehensive perspective. Researchers and stakeholders can refer to or base their further analyses on this

information, which may require the support of futher information about LULC. They can also adjust certain parameters of RFs to potentially improve classification accuracy. Additionally, they can apply PCA tests to other areas in combination with other regression methods.

## AUTHOR CONTRIBUTIONS

L.T. contributed to the conceptualization, methodology, software development, visualization of this research, and wrote the original draft. Z.Z. contributed to the resources and data curation selection, and supervised this work. R.T.L.K. participated in writing the original draft and reviewed and edited the manuscript.

## DATA AVAILABILITY STATEMENT

Data cannot be made publicly available; readers should contact the corresponding author for details.

## CONFLICT OF INTEREST

The authors declare there is no conflict.

## REFERENCES

Abdel-Rahman, E. M., Mutanga, O., Adam, E. & Ismail, R. 2014 Detecting Sirex noctilio grey-attacked and lightning-struck pine trees using airborne hyperspectral data, random forest and support vector machines classifiers. *ISPRS Journal of Photogrammetry and Remote Sensing* **88**, 48–59.

Adam, A. G. 2019 Thinking outside the box and introducing land readjustment against the conventional urban land acquisition and delivery method in Ethiopia. *Land Use Policy* **81**, 624–631.

Arifasihati, Y. 2016 Analysis of land use and cover changes in Ciliwung and Cisadane watershed in three decades. *Procedia Environmental Sciences* **33**, 465–469.

Breiman, L. 2001 Random forests. *Machine Learning* **45**, 5–32.

Briassoulis, H. & van der Straaten, J. 2000 Tourism and the environment: An overview. In: *Tourism and the Environment: Regional, Economic, Cultural and Policy Issues* (Briassoulis, H., van der Straaten, J., eds.), pp. 1–19.

Chen, J., He, C. & Yue, C. 2011 Atmospheric correction of an advance land imager (ALI) image based on the FLAASH module. *Journal of Zhejiang A&F University* **28**, 590–596.

Congalton, R. G. 1991 A review of assessing the accuracy of classifications of remotely sensed data. *Remote Sensing of Environment* **37**, 35–46.

Dai, E., Wu, Z. & Du, X. 2018 A gradient analysis on urban sprawl and urban landscape pattern between 1985 and 2000 in the Pearl River Delta, China. *Frontiers of Earth Science* **12**, 791–807.

Debnath, J., Sahariah, D., Lahon, D., Nath, N., Chand, K., Meraj, G., Farooq, M., Kumar, P., Kanga, S. & Singh, S. K. 2022 Geospatial modeling to assess the past and future land use-land cover changes in the Brahmaputra Valley, NE India, for sustainable land resource management. *Environmental Science and Pollution Research* 1–24.

De la Luz Hernández-Flores, M., Otazo-Sánchez, E. M., Galeana-Pizana, M., Roldán-Cruz, E. I., Razo-Zárate, R., González-Ramírez, C. A., Galindo-Castillo, E. & Gordillo-Martínez, A. J. 2017 Urban driving forces and megacity expansion threats. Study case in the Mexico City periphery. *Habitat International* **64**, 109–122.

Deng, L., Liu, G. b. & Shangguan, Z. p. 2014 Land-use conversion and changing soil carbon stocks in China's 'Grain-for-Green' Program: A synthesis. *Global Change Biology* **20**, 3544–3556.

Dewan, A. M. & Yamaguchi, Y. 2009 Using remote sensing and GIS to detect and monitor land use and land cover change in Dhaka Metropolitan of Bangladesh during 1960–2005. *Environmental Monitoring and Assessment* **150**, 237–249.

Ding, H. & Shi, W. 2013 Land-use/land-cover change and its influence on surface temperature: A case study in Beijing City. *International Journal of Remote Sensing* **34**, 5503–5517.

Di Nunno, F., de Marinis, G. & Granata, F. 2023a Short-term forecasts of streamflow in the UK based on a novel hybrid artificial intelligence algorithm. *Scientific Reports* **13**, 7036.

Di Nunno, F., Zhu, S., Ptak, M., Sojka, M. & Granata, F. 2023b A stacked machine learning model for multi-step ahead prediction of lake surface water temperature. *Science of the Total Environment* **10** (890), 164323.

Di Nunno, F., Giudicianni, C., Creaco, E. & Granata, F. 2023c Multi-step ahead groundwater level forecasting in Grand Est, France: Comparison between stacked machine learning model and radial basis function neural network. *Groundwater for Sustainable Development* **23**, 101042.

Du, X., Jin, X., Yang, X., Yang, X. & Zhou, Y. 2014 Spatial pattern of land use change and its driving force in Jiangsu Province. *International Journal of Environmental Research and Public Health* **11**, 3215–3232.

Essien, E. & Cyrus, S. 2019 Detection of urban development in Uyo (Nigeria) using remote sensing. *Land* **8**, 102.

Feng, R. & Wang, K. 2021 Spatiotemporal effects of administrative division adjustment on urban expansion in China. *Land Use Policy* **101**, 105143.

Feng, R. & Wang, K. 2022 The direct and lag effects of administrative division adjustment on urban expansion patterns in Chinese mega-urban agglomerations. *Land Use Policy* **112**, 105805.

Gaur, S. & Singh, R. 2023 A comprehensive review on land use/land cover (LULC) change modeling for urban development: Current status and future prospects. *Sustainability* **15**, 903.

Ge, Y., Zhang, K. & Yang, X. 2019 A 110-year pollen record of land use and land cover changes in an anthropogenic watershed landscape, eastern China: Understanding past human-environment interactions. *Science of the Total Environment* **650**, 2906–2918.

Granata, F., Di Nunno, F. & de Marinis, G. 2022a Stacked machine learning algorithms and bidirectional long short-term memory networks for multi-step ahead streamflow forecasting: A comparative study. *Journal of Hydrology* **613** (1–4), 128431.

Granata, F., Di Nunno, F., Najafzadeh, M. & Demir, I. 2022b A stacked machine learning algorithm for multi-step ahead prediction of soil moisture. *Hydrology* **10** (1), 1–19.

Hastie, T., Tibshirani, R., Friedman, J. H. & Friedman, J. H. 2009 *The Elements of Statistical Learning: Data Mining, Inference, and Prediction*, Vol. 2. Springer, New York, NY.

Hersperger, A. M. & Bürgi, M. 2009 Going beyond landscape change description: Quantifying the importance of driving forces of landscape change in a Central Europe case study. *Land Use Policy* **26**, 640–648.

Hietel, E., Waldhardt, R. & Otte, A. 2004 Analysing land-cover changes in relation to environmental variables in Hesse, Germany. *Landscape Ecology* **19**, 473–489.

Islam, M. D., Islam, K. S., Ahasan, R., Mia, M. R. & Haque, M. E. 2021 A data-driven machine learning-based approach for urban land cover change modeling: A case of Khulna City Corporation area. *Remote Sensing Applications: Society and Environment* **24**, 100634.

Jin, X., Jiang, P., Ma, D. & Li, M. 2019 Land system evolution of Qinghai-Tibetan Plateau under various development strategies. *Applied Geography* **104**, 1–9.

Jiyuan, L., Mingliang, L., Xiangzheng, D., Dafang, Z., Zengxiang, Z. & Di, L. 2002 The land use and land cover change database and its relative studies in China. *Journal of Geographical Sciences* **12**, 275–282.

Jolliffe, I. T. & Cadima, J. 2016 Principal component analysis: A review and recent developments. *Philosophical Transactions of the Royal Society A: Mathematical, Physical and Engineering Sciences* **374**, 20150202.

Kontgis, C., Schneider, A., Fox, J., Saksena, S., Spencer, J. H. & Castrence, M. 2014 Monitoring peri-urbanization in the greater Ho Chi Minh City metropolitan area. *Applied Geography* **53**, 377–388.

Lawler, J. J., Lewis, D. J., Nelson, E., Plantinga, A. J., Polasky, S., Withey, J. C., Helmers, D. P., Martinuzzi, S., Pennington, D. & Radeloff, V. C. 2014 Projected land-use change impacts on ecosystem services in the United States. *Proceedings of the National Academy of Sciences* **111**, 7492–7497.

Li, X., Chen, W., Cheng, X. & Wang, L. 2016 A comparison of machine learning algorithms for mapping of complex surface-mined and agricultural landscapes using ZiYuan-3 stereo satellite imagery. *Remote Sensing* **8**, 514.

Li, J., Wang, Z., Lai, C., Wu, X., Zeng, Z., Chen, X. & Lian, Y. 2018 Response of net primary production to land use and land cover change in mainland China since the late 1980s. *Science of the Total Environment* **639**, 237–247.

Li, M., Zhou, Y., Xiao, P., Tian, Y., Huang, H. & Xiao, L. 2021 Evolution of habitat quality and its topographic gradient effect in Northwest Hubei Province from 2000 to 2020 based on the InVEST model. *Land* **10**, 857.

Lu, D., Li, G., Moran, E., Dutra, L. & Batistella, M. 2011 A comparison of multisensor integration methods for land cover classification in the Brazilian Amazon. *GIScience & Remote Sensing* **48**, 345–370.

Maxwell, A. E., Strager, M. P., Warner, T. A., Ramezan, C. A., Morgan, A. N. & Pauley, C. E. 2019 Large-area, high spatial resolution land cover mapping using random forests, GEOBIA, and NAIP orthophotography: Findings and recommendations. *Remote Sensing* **11**, 1409.

Millard, K. & Richardson, M. 2015 On the importance of training data sample selection in random forest image classification: A case study in peatland ecosystem mapping. *Remote Sensing* **7**, 8489–8515.

Mooney, H. A., Duraiappah, A. & Larigauderie, A. 2013 Evolution of natural and social science interactions in global change research programs. *Proceedings of the National Academy of Sciences* **110**, 3665–3672.

Nagy, R. C. & Lockaby, B. G. 2011 Urbanization in the Southeastern United States: Socioeconomic forces and ecological responses along an urban-rural gradient. *Urban Ecosystems* **14**, 71–86.

Nassar, A. K., Blackburn, G. A. & Whyatt, J. D. 2014 Developing the desert: The pace and process of urban growth in Dubai. *Computers, Environment and Urban Systems* **45**, 50–62.

Pourazar, H., Samadzadegan, F. & Dadrass Javan, F. 2019 Aerial multispectral imagery for plant disease detection: Radiometric calibration necessity assessment. *European Journal of Remote Sensing* **52**, 17–31.

Rawat, J. & Kumar, M. 2015 Monitoring land use/cover change using remote sensing and GIS techniques: A case study of Hawalbagh block, district Almora, Uttarakhand, India. *The Egyptian Journal of Remote Sensing and Space Science* **18**, 77–84.

Rodriguez-Galiano, V. F. & Chica-Rivas, M. 2014 Evaluation of different machine learning methods for land cover mapping of a Mediterranean area using multi-seasonal Landsat images and Digital Terrain Models. *International Journal of Digital Earth* **7**, 492–509.

Sánchez-Cuervo, A. M., Aide, T. M., Clark, M. L. & Etter, A. 2012 Land cover change in Colombia: Surprising forest recovery trends between 2001 and 2010, PLOS One.

Sanderson, E. W., Jaiteh, M., Levy, M. A., Redford, K. H., Wannebo, A. V. & Woolmer, G. 2002 The human footprint and the last of the wild: The human footprint is a global map of human influence on the land surface, which suggests that human beings are stewards of nature, whether we like it or not. *BioScience* **52**, 891–904.

Schoeman, F., Newby, T., Thompson, M. & Van den Berg, E. C. 2013 South African national land-cover change map. *South African Journal of Geomatics* **2**, 94–105.

Shao, Y. & Lunetta, R. S. 2012 Comparison of support vector machine, neural network, and CART algorithms for the land-cover classification using limited training data points. *ISPRS Journal of Photogrammetry and Remote Sensing* **70**, 78–87.

Speiser, J. L., Miller, M. E., Tooze, J. & Ip, E. 2019 A comparison of random forest variable selection methods for classification prediction modeling. *Expert Systems with Applications* **134**, 93–101.

Stephen, D., David, J. & Anand, P. 1993 Conflicting interests in the use of Kerala's penaeid shrimp resources: A case in question. *Journal of the Marine Biological Association of India* **35**, 29–38.

Sun, L., Wei, J., Duan, D., Guo, Y., Yang, D., Jia, C. & Mi, X. 2016 Impact of land-use and land-cover change on urban air quality in representative cities of China. *Journal of Atmospheric and Solar-Terrestrial Physics* **142**, 43–54.

Tadese, M., Kumar, L., Koech, R. & Kogo, B. K. 2020 Mapping of land-use/land-cover changes and its dynamics in Awash River Basin using remote sensing and GIS. *Remote Sensing Applications: Society and Environment* **19**, 100352.

Tavares, A. O., Monteiro, M., Barros, J. L. & Santos, P. P. 2019 Long-term land-use changes in small/medium-sized cities. Enhancing the general trends and local characteristics. *European Planning Studies* **27**, 1432–1459.

Teluguntla, P., Thenkabail, P. S., Oliphant, A., Xiong, J., Gumma, M. K., Congalton, R. G., Yadav, K. & Huete, A. 2018 A 30-m landsat-derived cropland extent product of Australia and China using random forest machine learning algorithm on Google Earth Engine cloud computing platform. *ISPRS: Journal of Photogrammetry and Remote Sensing* **144**, 325–340.

Tendaupenyu, P., Magadza, C. H. D. & Murwira, A. 2017 Changes in landuse/landcover patterns and human population growth in the Lake Chivero catchment, Zimbabwe. *Geocarto International* **32**, 797–811.

Thanh Noi, P. & Kappas, M. 2017 Comparison of random forest, k-nearest neighbor, and support vector machine classifiers for land cover classification using Sentinel-2 imagery. *Sensors* **18**, 18.

Tian, Y., Yin, K., Lu, D., Hua, L., Zhao, Q. & Wen, M. 2014 Examining land use and land cover spatiotemporal change and driving forces in Beijing from 1978 to 2010. *Remote Sensing* **6**, 10593–10611.

Tiitu, M. 2018 Expansion of the built-up areas in Finnish city regions – The approach of travel-related urban zones. *Applied Geography* **101**, 1–13.

Toure, S. I., Stow, D. A., Shih, H.-c., Weeks, J. & Lopez-Carr, D. 2018 Land cover and land use change analysis using multi-spatial resolution data and object-based image analysis. *Remote Sensing of Environment* **210**, 259–268.

Turner, R. K., Adger, W. N. & Doktor, N. 1993 *Key issues in the economics of sea level rise*. Centre for Social and Economic Research on the Global Environment. CSERGE Working Paper PA 93-04 The Centre for Social and Economic Research on the Global Environment (CSERGE) is a designated research centre of the U.K. Economic and Social Research Council (ESRC). ISSN 0967-8875.

Van Asselen, S. & Verburg, P. H. 2013 Land cover change or land-use intensification: Simulating land system change with a global-scale land change model. *Global Change Biology* **19**, 3648–3667.

Van Beijma, S., Comber, A. & Lamb, A. 2014 Random forest classification of salt marsh vegetation habitats using quad-polarimetric airborne SAR, elevation and optical RS data. *Remote Sensing of Environment* **149**, 118–129.

Van der Linden, S., Rabe, A., Held, M., Jakimow, B., Leitão, P. J., Okujeni, A., Schwieder, M., Suess, S. & Hostert, P. 2015 The EnMAP-Box – A toolbox and application programming interface for EnMAP data processing. *Remote Sensing* **7**, 11249–11266.

Voss, M. & Sugumaran, R. 2008 Seasonal effect on tree species classification in an urban environment using hyperspectral data, LiDAR, and an object-oriented approach. *Sensors* **8**, 3020–3036.

Wang, Z.-J., Liu, S.-J., Li, J.-H., Pan, C., Wu, J.-L., Ran, J. & Su, Y. 2022 Remarkable improvement of ecosystem service values promoted by land use/land cover changes on the Yungui Plateau of China during 2001–2020. *Ecological Indicators* **142**, 109303.

Wear, D. N. & Bolstad, P. 1998 Land-use changes in southern Appalachian landscapes: Spatial analysis and forecast evaluation. *Ecosystems* **1**, 575–594.

Whiteside, H. 2020 Privatizing Canadian government land and real estate: Railroads, reconciliation, and rip-offs. *Land Use Policy* **99**, 104821.

Wu, Q., Li, H.-q., Wang, R.-s., Paulussen, J., He, Y., Wang, M., Wang, B.-h. & Wang, Z. 2006 Monitoring and predicting land use change in Beijing using remote sensing and GIS. *Landscape and Urban Planning* **78**, 322–333.

Wu, Y., Li, S. & Yu, S. 2016 Monitoring urban expansion and its effects on land use and land cover changes in Guangzhou city, China. *Environmental Monitoring and Assessment* **188**, 1–15.

Wulder, M. A., White, J. C., Goward, S. N., Masek, J. G., Irons, J. R., Herold, M., Cohen, W. B., Loveland, T. R. & Woodcock, C. E. 2008 Landsat continuity: Issues and opportunities for land cover monitoring. *Remote Sensing of Environment* **112**, 955–969.

Xie, Y., Mei, Y., Guangjin, T. & Xuerong, X. 2005 Socio-economic driving forces of arable land conversion: A case study of Wuxian City, China. *Global Environmental Change* **15**, 238–252.

Xu, Y., McNamara, P., Wu, Y. & Dong, Y. 2013 An econometric analysis of changes in arable land utilization using multinomial logit model in Pinggu district, Beijing, China. *Journal of Environmental Management* **128**, 324–334.

Yao, Z., Wang, B., Huang, J., Zhang, Y., Yang, J., Deng, R. & Yang, Q. 2021 Analysis of land use changes and driving forces in the Yanhe River Basin from 1980 to 2015. *Journal of Sensors* **2021**, 1–11.

Yin, J., Yin, Z., Zhong, H., Xu, S., Hu, X., Wang, J. & Wu, J. 2011 Monitoring urban expansion and land use/land cover changes of Shanghai metropolitan area during the transitional economy (1979–2009) in China. *Environmental Monitoring and Assessment* **177**, 609–621.

Yu, X. & Yang, G. 2002 The advances and problems of land use and land cover change research in China. *Progress in Geography* **21**, 51–57.

Zhang, S., De Roo, G. & Van Dijk, T. 2015 Urban land changes as the interaction between self-organization and institutions. *Planning Practice and Research* **30**, 160–178.

Zhang, D., Wang, X., Qu, L., Li, S., Lin, Y., Yao, R., Zhou, X. & Li, J. 2020 Land use/cover predictions incorporating ecological security for the Yangtze River Delta region, China. *Ecological Indicators* **119**, 106841.

Zhou, Y., Li, Y. & Xu, C. 2020 Land consolidation and rural revitalization in China: Mechanisms and paths. *Land Use Policy* **91**, 104379.

Zhu, Z. & Woodcock, C. E. 2014 Continuous change detection and classification of land cover using all available Landsat data. *Remote Sensing of Environment* **144**, 152–171.

Zhu, L., Song, R., Sun, S., Li, Y. & Hu, K. 2022 Land use/land cover change and its impact on ecosystem carbon storage in coastal areas of China from 1980 to 2050. *Ecological Indicators* **142**, 109178.

First received 29 November 2023; accepted in revised form 26 December 2023. Available online 6 February 2024